Draft version July 20, 2021
Typeset using LaTeX **twocolumn** style in AASTeX631

A Search for Circumstellar Companions Around Nearby White Dwarf Sirius b

Miles Lucas [1], Michael Bottom [1], Garreth Ruane [2], and Sam Ragland [3]

[1] *Institute for Astronomy, University of Hawai'i, USA*
[2] *Jet Propulsion Laboratory, California Institute of Technology, USA*
[3] *W.M. Keck Observatory, USA*

ABSTRACT

1. INTRODUCTION

Very little is known about the evolution of planetary systems beyond the main-sequence lifetime of their host stars. Theoretical calculations show that planets can survive the red giant and asymptotic giant stages (Burleigh et al. 2002; Jura 2008; Nordhaus & Spiegel 2013), and results from radial velocity and transit surveys suggest extrasolar planets are prevalent throughout the Milky Way (Cumming et al. 2008). However, only one planetary mass object has been detected around a white dwarf (WD) with imaging (WD 0806-661; Luhman et al. 2011).

Directly imaging exoplanets is a powerful method in exoplanet science which explores a parameter space very complementary to the popular transit photometry and radial velocity methods. The red giant stage has cleared planets within a few au greatly lowering the transit probability. White dwarfs have very few spectral lines to make high-precision radial velocity measurements from spectral lines. Imaging, though, benefits from the orbital expansion of the planet, and the cooling of the white dwarf greatly reduces the contrast between them (Burleigh et al. 2002; Gould & Kilic 2008). The Degenerate Objects around Degenerate Objects (DODO) survey observed 29 white dwarfs with Gemini/NIRI and VLT/ISAAC and provided upper limits around $\sim$8 M_J beyond 35 AU (Hogan et al. 2009).

In this work we study the closest white dwarf to the Sun, Sirius b, and provide upper mass limits based on our observations in the near-infrared. section 2 describes our target and observing strategy, section 3 describes the processing and analysis techniques used, section 4 describes our results and we conclude with section 5.

2. OBSERVATIONS

Sirius is the closest star system to the Sun at 2.7 pc away, consisting of an A1Vm star (a) and a WD with an age around 225 Myr (Bond et al. 2017; Collaboration et al. 2018). There are no known planets around either star, and using constrained 3-body numerical simulations a potential companion around Sirius b would only be stable with a 1.79 yr orbit, which corresponds to a circular orbit with 1.5 AU separation. Sirius b has been studied in the 10 µm regime recently by Pathak et al. (2021), who achieve 1.8 M_J to 3.5 M_J upper limits within 2 arcseconds.

We targeted Sirius b directly using Keck/NIRC2 in Lp-band across three epochs in 2020 Table 1. Due to the high proper motion and reasonable orbital motion, we started by calculating the projected offset and position angle from Sirius a based on the orbital parameters from Bond et al. (2017). We first slewed to Sirius a, which is easy to lock onto due to its brightness (-1.35 K-band magnitude; Bonnet-Bidaud & Pantin 2008). We found that Sirius b is too dim (9.01 K-band magnitude; Bonnet-Bidaud & Pantin 2008) for the adaptive optics (AO) performance necessary for coronagraphy and that the scattered light from Sirius a was detrimental to closing the AO loop when using Sirius b as a natural guide star (NGS) anyways. Therefore, we employed a unique off-axis solution, using a narrow laser-line filter for the wavefront sensor using Sirius a as the NGS and offsetting to Sirius b manually.

The scattered light from Sirius a is so strong, in fact, that radial diffraction spikes from the Keck II secondary mirror support structure are still present in the Sirius b frames, which reduced our overall observing efficiency due to discarding these frames. An example of such a diffraction spike is shown in Figure 1.

3. ANALYSIS

Corresponding author: Miles Lucas
mdlucas@hawaii.edu

Table 1. Observing parameters for the three epochs of data. All observations were carried out using the NIRC2 Lp-band filter. Observation time is based on the frames that were selected for processing.

Date observed	Sirius a offset (")	Sirius a PA (°)	Observation time (hr)	Seeing (arcsec)	Temp (°C)	PWV (mm)
2020-02-04	11.20	67.90	1.44			
2020-11-21	11.27	66.42	2.91			
2020-11-28	11.27	66.38	2.44			

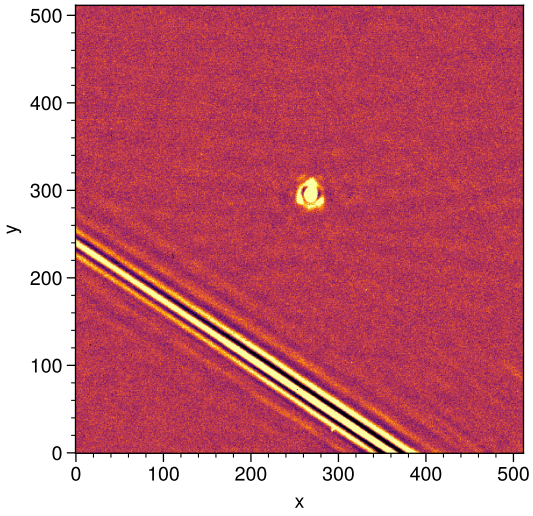

Figure 1. Calibrated science frame of Sirius b from 2020-02-04 epoch showing the strong scattered light effects from Sirius a.

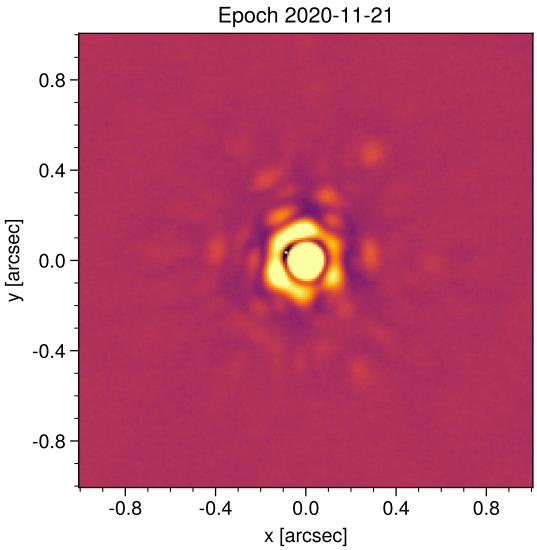

Figure 2. The median frame from the 2020-11-21 epoch showing the instrumental PSF. The inner core has a FWHM of ∼76 mas. The speckle pattern can be seen in the blobs surrounding the first ring, with roughly 6-way radial symmetry corresponding to the hexagonal shapes of the segmented mirrors.

For each epoch we applied a flat correction using calibration frames captured during observing. We also removed bad pixels using a combination of L.A.Cosmic (Dokkum & G 2001) and an adaptive sigma-clipping algorithm. We finally remove sky background using a high-pass median filter. At this point frames were manually filtered to remove bad frames, especially those with diffraction spikes like in Figure 1. Then, each good frame is co-registered using cross-correlations (Guizar-Sicairos et al. 2008) and aligned with the center of the FOV. Lastly the frames were cropped to the inner 200 pixels and stacked into data cubes for each epoch. With the pixel scale of 10 mas/px the crop corresponds to a maximum separation of 2.7 AU. We also measure the parallactic angle of each frame, including corrections for distortion effects following Yelda et al. (2010). For each epoch, we measure the full-width at half-maximum (FWHM) of the stellar PSF by fitting a bivariate Gaussian model to the median frame from each data cube (an example of one is shown in Figure 2).

During observing we applied the technique of angular differential imaging (ADI; Marois et al. 2006) where we disable the field rotator and allow the FOV to rotate throughout the night along with Earth. The point-spread function (PSF), which is an instrumental effect, will not appear to rotate while any potential companion will appear to rotate. This allows modeling and subtracting the PSF with less probability for subtracting companion signal. After subtraction, the frames are derotated by their parallactic angle and combined with a weighted sum (Bottom et al. 2017), which reduces the pixel-to-pixel noise as the number of frames in the data cube increases.

For this analysis we used three statistical models for modeling the stellar PSF, classic median subtraction (Marois et al. 2006), principal component analysis (PCA; Soummer et al. 2012), and fixed-point greedy disk subtraction (GreeDS; Pairet et al. 2019b, 2020). The median subtraction and PCA methods were also applied in an annular method, where we model the PSF in annuli of increasing separation, since each annulus

has similar statistcal properties under the framework of ADI (Marois et al. 2006).

We used three metrics for determining the performance of each algorithm, the signal-to-noise ratio (S/N) detection map, the standardized trajectory intensity mean map (STIM map; Pairet et al. 2019a), and the STIM largest intensity mask map (SLIM map; Pairet 2020). These metrics assign a likelihood to each pixel for the presence of a companion using different assumptions of the residual statistics. The SLIM map is an ensemble statistic which calculates the average STIM map from many residual cubes, such as many variations of PCA with differing number of components.

Another metric we calculate for some of the algorithms is the contrast curve, which determines the sensitivity of a 5σ statistical detection through repeated injection and retrieval of planetary signal as processed by one of the ADI algorithms above. We calculate both the Gaussian contrast and the Student-t corrected contrast, which accounts for the small-sample statistics in each annulus (Mawet et al. 2014).

4. RESULTS

The best performing algorithms for each epoch in terms of sensitivity were median subtraction median subtraction, and PCA subtraction with 2 principal components. The flat residual images from each epoch are shown in Figure 3, along with the Gaussian S/N maps (Figure 4) and STIM maps (Figure 5). For each epoch we determined there was not significant evidence for a companion around Sirius b.

5. CONCLUSIONS

Software: ADI.jl (Lucas & Bottom 2020), astropy (Collaboration et al. 2013; Astropy Collaboration et al. 2018), Julia (Bezanson et al. 2017), numpy (Harris et al. 2020), scikit-image (Walt et al. 2014),

REFERENCES

Astropy Collaboration, Price-Whelan, A. M., Sipőcz, B. M., et al. 2018, The Astronomical Journal, 156, 123, doi: 10.3847/1538-3881/aabc4f

Bezanson, J., Edelman, A., Karpinski, S., & Shah, V. B. 2017, SIAM Rev., 59, 65, doi: 10.1137/141000671

Bond, H. E., Schaefer, G. H., Gilliland, R. L., et al. 2017, The Astrophysical Journal, 840, 70, doi: 10.3847/1538-4357/aa6af8

Bonnet-Bidaud, J.-M., & Pantin, E. 2008, A&A, 489, 651, doi: 10.1051/0004-6361:20078937

Bottom, M., Ruane, G., & Mawet, D. 2017, Research Notes of the American Astronomical Society, 1, 30, doi: 10.3847/2515-5172/aa9d18

Burleigh, M. R., Clarke, F. J., & Hodgkin, S. T. 2002, Monthly Notices of the Royal Astronomical Society, 331, L41, doi: 10.1046/j.1365-8711.2002.05417.x

Collaboration, A., Robitaille, T. P., Tollerud, E. J., et al. 2013, Astronomy and Astrophysics, 558, A33, doi: 10.1051/0004-6361/201322068

Collaboration, G., Brown, A. G. A., Vallenari, A., et al. 2018, Astronomy & Astrophysics, Volume 616, id.A1, <NUMPAGES>22</NUMPAGES> pp., 616, A1, doi: 10.1051/0004-6361/201833051

Cumming, A., Butler, R. P., Marcy, G. W., et al. 2008, Publications of the Astronomical Society of the Pacific, 120, 531, doi: 10.1086/588487

Dokkum, V., & G, P. 2001, Publications of the Astronomical Society of the Pacific, 113, 1420, doi: 10.1086/323894

Gould, A., & Kilic, M. 2008, The Astrophysical Journal, 673, L75, doi: 10.1086/527476

Guizar-Sicairos, M., Thurman, S. T., & Fienup, J. R. 2008, Opt. Lett., OL, 33, 156, doi: 10.1364/OL.33.000156

Harris, C. R., Millman, K. J., van der Walt, S. J., et al. 2020, Nature, 585, 357, doi: 10.1038/s41586-020-2649-2

Hogan, E., Burleigh, M. R., & Clarke, F. J. 2009, Monthly Notices of the Royal Astronomical Society, 396, 2074, doi: 10.1111/j.1365-2966.2009.14565.x

Jura, M. 2008, The Astronomical Journal, 135, 1785, doi: 10.1088/0004-6256/135/5/1785

Lucas, M., & Bottom, M. 2020, Journal of Open Source Software, 5, 2843, doi: 10.21105/joss.02843

Luhman, K. L., Burgasser, A. J., & Bochanski, J. J. 2011, The Astrophysical Journal, 730, L9, doi: 10.1088/2041-8205/730/1/L9

Marois, C., Lafrenière, D., Doyon, R., Macintosh, B., & Nadeau, D. 2006, The Astrophysical Journal, 641, 556, doi: 10.1086/500401

Mawet, D., Milli, J., Wahhaj, Z., et al. 2014, ApJ, 792, 97, doi: 10.1088/0004-637X/792/2/97

Nordhaus, J., & Spiegel, D. S. 2013, Monthly Notices of the Royal Astronomical Society, 432, 500, doi: 10.1093/mnras/stt569

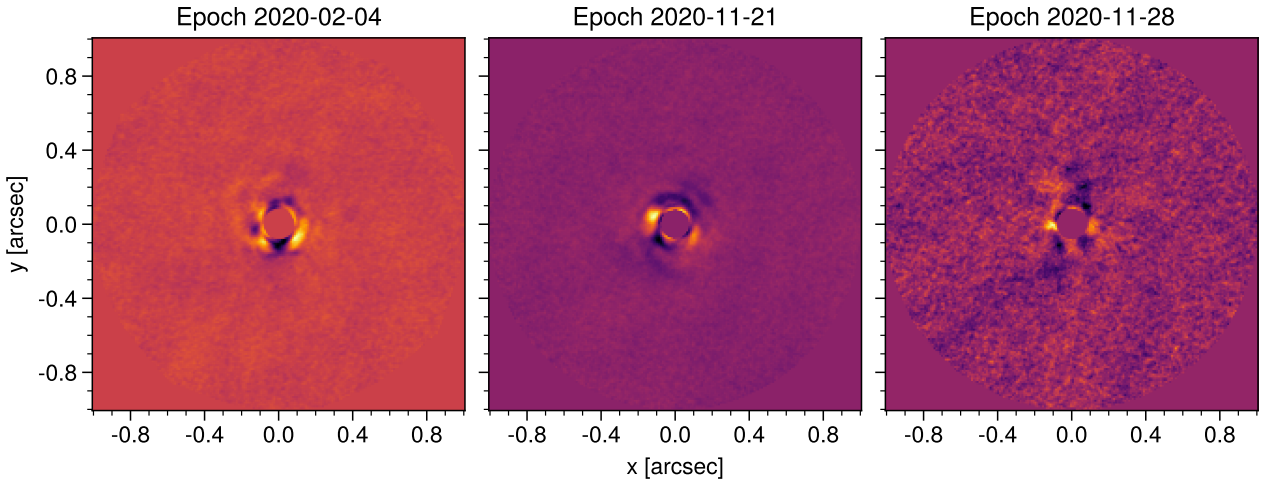

Figure 3. The flat residuals of each epoch after PSF subtraction, derotating, and collapsing. The inner full-width at half-maximum (FWHM) is masked out for each frame.

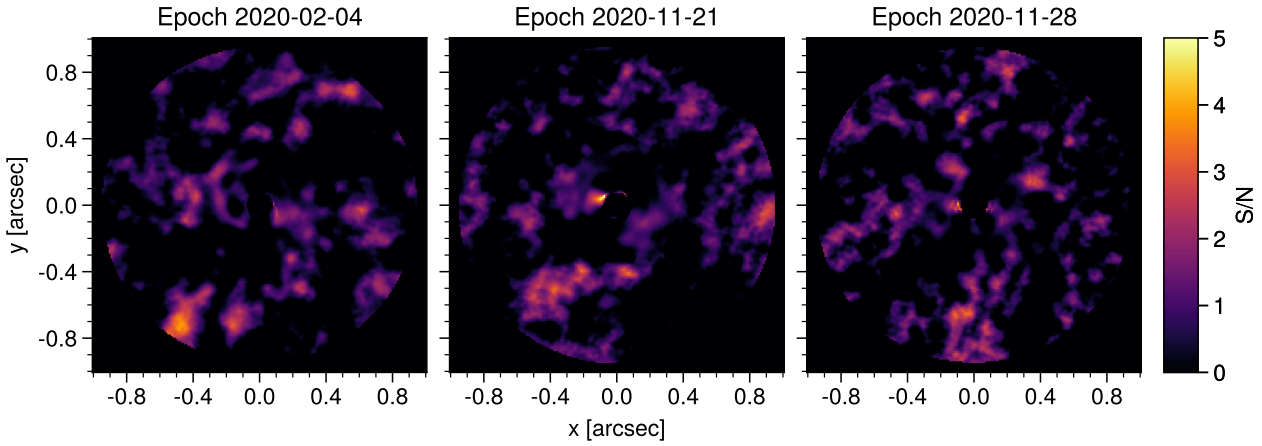

Figure 4. The S/N maps for each epoch calculated with Gaussian noise assumptions. The inner full-width at half-maximum (FWHM) is masked out for each map.

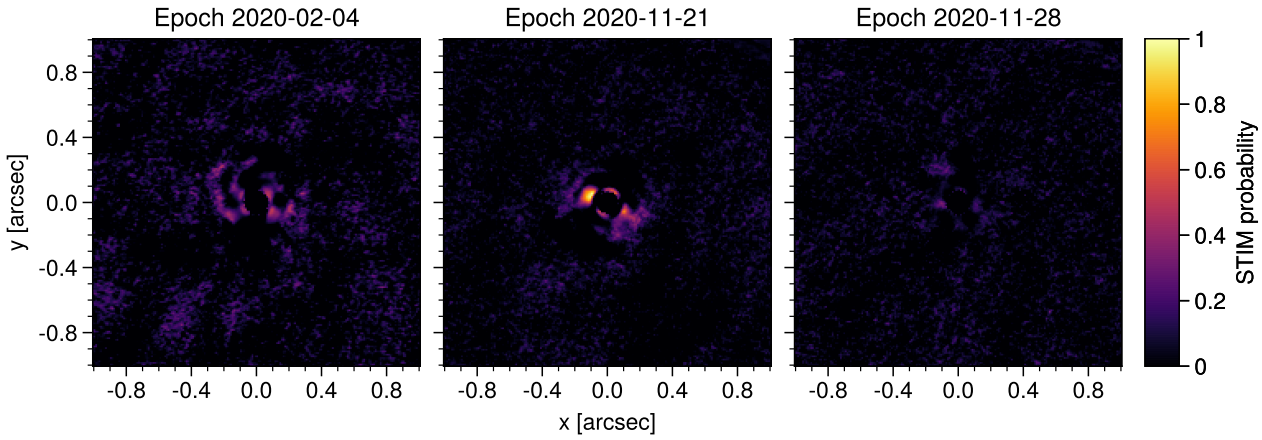

Figure 5. The STIM maps for each epoch calculated from the residual cube. Note that the STIM probability has a typical cutoff threshold of 0.5 for significant detections. The inner full-width at half-maximum (FWHM) is masked out for each map.

Pairet, B. 2020, PhD thesis, UCL - Université Catholique de Louvain. https://dial.uclouvain.be/pr/boreal/object/boreal:240621

Pairet, B., Cantalloube, F., Gomez Gonzalez, C. A., Absil, O., & Jacques, L. 2019a, Monthly Notices of the Royal Astronomical Society, 487, 2262, doi: 10.1093/mnras/stz1350

Pairet, B., Cantalloube, F., & Jacques, L. 2019b, arXiv:1812.01333 [astro-ph]. http://arxiv.org/abs/1812.01333

—. 2020, arXiv:2008.05170 [astro-ph]. http://arxiv.org/abs/2008.05170

Pathak, P., de la Roche, D. J. M. P. d., Kasper, M., et al. 2021, arXiv:2104.13032 [astro-ph]. http://arxiv.org/abs/2104.13032

Soummer, R., Pueyo, L., & Larkin, J. 2012, The Astrophysical Journal Letters, 755, L28, doi: 10.1088/2041-8205/755/2/L28

Walt, S. v. d., Schönberger, J. L., Nunez-Iglesias, J., et al. 2014, PeerJ, 2, e453, doi: 10.7717/peerj.453

Yelda, S., Lu, J. R., Ghez, A. M., et al. 2010, The Astrophysical Journal, Volume 725, Issue 1, pp. 331-352 (2010)., 725, 331, doi: 10.1088/0004-637X/725/1/331